

**United States
Department of
Agriculture**

**Natural Resources
Conservation
Service**

**11 Campus Boulevard,
Suite 200
Newtown Square, PA 19073**

Subject: SOI – Geophysical Field Assistance

Date: 5 June 2009

To: Dr. Jeffrey McDonnell
Department of Forest Engineering
015 Peavy Hall
Oregon State University
Corvallis, Oregon 97331-5706

Chad McGrath
State Soil Scientist
USDA-Natural Resources Conservation Service
Suite 900
1201 NE Lloyd Blvd.
Portland, OR 97232

Purpose:

During this field trip, ground-penetrating radar (GPR) traverses were completed within the Aalsea (Lincoln County) and H. J. Andrews (Lane County) Watersheds in western Oregon. These GPR surveys sought to: 1) delineate the interface separating soil and competent bedrock; 2) characterize the orientation of cracks and/or fractures in bedrock; and 3) determine presence/absence of vertical/horizontal preferential flowpaths in saprolite/bedrock. In addition, this study sought to improve protocol for conducting geophysical investigations in very-steeply sloping, densely-forested watersheds.

Participants:

Jim Doolittle, Research Soil Scientist, USDA-NRCS-NSSC, Newtown Square, PA
Rosemary Fanelli, PhD student, Department of Forest Engineering, Resources and Management, Oregon State University, Corvallis, OR
Chris Gabrielli, MS student, Water Resource Engineering graduate program, Oregon State University, Corvallis, OR
Landon Gryczkowski, MS student, Department of Biological and Ecological Engineering, Oregon State University, Corvallis, OR
Cody Hale, PhD student, Department of Forest Engineering, Resources and Management, Oregon State University, Corvallis, OR
Luisa Hopp, Postdoc, Department of Forest Engineering, Resources and Management, Oregon State University, Corvallis, OR
Jeffrey McDonnell, Professor & Richardson Chair in Watershed Science, Department of Forest Engineering, Oregon State University, Corvallis, OR
Travis Roth, PhD student, Biological and Ecological Engineering, Oregon State University, Corvallis, OR
Takahiro Sayama, Postdoc, Department of Forest Engineering, Resources and Management, Oregon State University, Corvallis, OR

Activities:

All field activities were completed on 4 and 8 May 2008.

Summary:

1. Multiple GPR traverses were conducted along nineteen traverse lines that are located on different slope components in two watersheds: the Aalsea Watershed and Watershed 10. Traverses were completed with a 200

MHz antenna, which provided satisfactory penetration depths and moderate resolution of subsurface features. Along each traverse line, flagged reference points were spaced at intervals of either 2 or 3-m. Along each traverse line, the relative elevations of these reference points were measured with an engineering level. These measurements were used to “terrain correct” the radar records for improved visualizations and interpretations.

2. In the absence of ground-truth, radar records discussed in this report can not be interpreted unequivocally. All depth scales used in this report are approximation based on soil conditions and the velocity of propagation of the radar pulse through the upper 50 cm of the soil profile.
3. Using a 200 MHz antenna, soil and bedrock were profiled to estimated depths of about 5 m. Subsurface reflection patterns were highly complex and spatially variable. This variability occurred over surprisingly short distances. While the soil-bedrock interface could be interpreted with some degree of certainty, weathering zones within the parent rock were difficult to identify with any degree of confidence. Interpretations can be improved if properly verified with ground truth cores and observations. While present GPR records do not provide a unique solution, they may help to improve broad interpretations and models of these watersheds.
4. Though unconfirmed, GPR may be used to detect and characterize some fractures and preferential flow paths in soils and rocks of these watersheds. It is believed that constructive and destructive interference of the radar waveforms (caused by small-scale heterogeneities and truncated bedrock layers) is partially responsible for the segmentation of subsurface interfaces and the appearance of tortuous, white-colored, downward descending patterns on the radar records. These patterns suggest fractures and may represent preferential flowpaths in the underlying saprolite and unweathered bedrock. Additional studies are needed to determine the validity of these interpretations.
5. Surface normalized radar records from this study have been prepared into bitmap images and mailed to Dr McDonnell. In subsequent months, the radar records will be further reviewed and analyzed by his students.

It was my pleasure to participate in this study and to conduct fieldwork with you and your graduate students at Oregon State University.

With kind regards,

James A. Doolittle
 Research Soil Scientist
 National Soil Survey Center

cc:

- K. Hipple, Acting Director, National Soil Survey Center, USDA-NRCS, Federal Building, Room 152, 100 Centennial Mall North, Lincoln, NE 68508-3866
- M. Golden, Director of Soils Survey Division, USDA-NRCS, Room 4250 South Building, 14th & Independence Ave. SW, Washington, DC 20250
- Tuttle, Soil Scientist (Geophysical), National Soil Survey Center, USDA-NRCS, P.O. Box 60, 207 West Main Street, Rm. G-08, Federal Building, Wilkesboro, NC 28697
- L. West, National Leader, Soil Survey Research and Laboratory Staff, National Soil Survey Center, USDA-NRCS, Federal Building, Room 152, 100 Centennial Mall North, Lincoln, NE 68508-3866

Study Area:

Alsea Watershed:

This watershed (about 44.520 N. Latitude, 123.855 W. Longitude) is formed by a tributary to the Alsea River and is located within the Coastal Range in Lincoln County, Oregon. The Alsea Watershed provides an opportunity to compare the response of soil and water resources to current forest practices with those resulting from an extreme manipulation in the 1960s. Changes in discharge, sediment, and nutrients are being monitored. The watershed is located within an area of Bohannon gravelly loam, 37 to 50 % slopes (BmF). The moderately deep, well drained Bohannon soils formed in loamy colluvium and residuum weathered from andesite, arkosic sandstone, or other sedimentary rock types on mountain slopes. Bohannon soils form on metastable to active landforms, which are typified by uneven, step-like benches caused by sliding and slumping of bedrock, which reflect ongoing erosional processes.

Watershed #10:

Watershed # 10 (about 44.213 N Latitude., 122.262 W. Longitude) is formed by a tributary to the Blue River and is located in the Western Cascades in Lane County, Oregon. The watershed, which is about 10.2 hectares in size and at elevations ranging from 430 to 670 m, was clear-cut in 1975. The watershed is located within the H. J. Andrews Experimental Forest, Willamette National Forest. Soils have not been mapped within the National Forest. On nearby, similar landscapes in Lane County, Kinney and Klickitat soils are mapped. The deep, well drained Kinney soils formed in colluvium and residuum weathered from igneous tuffaceous agglomerate on ridge tops and side slopes of uplands. Depth to a paralithic contact (saprolite; Cr horizon) ranges from 100 to 150 cm or more. The 25 to 100 cm control section of Kinney soils averages 5 to 35 percent rock fragments and 22 to 35 percent clay. The deep, well drained Klickitat soils formed in colluvium and residuum weathered from basalt on uplands. Depth to highly fractured bedrock is 100 to 150 cm or more. Rock fragments of gravel and cobble size range from 15 to 70 percent in the solum and generally increase with depth. Both Kinney and Klickitat have an umbric epipedon, which ranges from 25 to 50 cm thick. Slopes range from 3 to 75 percent.

The taxonomic classifications of the aforementioned soils are listed in Table 1. These medium textured soils are considered to have a moderate potential for GPR investigations (<http://soils.usda.gov/survey/geography/maps/GPR/index.html>).

Table 1. Taxonomic Classification of Soils

Soil Series	Taxonomic Classification
Bohannon	fine-loamy, isotic, mesic Andic Dystrudepts
Kinney	Fine-loamy, isotic, mesic Andic Dystrudepts
Klickitat	Loamy-skeletal, isotic, mesic Humic Dystrudepts

Materials and Methods:

The radar unit is the TerraSIRch Subsurface Interface Radar (SIR) System-3000 (SIR-3000), manufactured by Geophysical Survey Systems, Inc. (GSSI; Salem, NH).¹ The SIR-3000 consists of a digital control unit (DC-3000) with keypad, SVGA video screen, and connector panel. A 10.8-volt lithium-ion rechargeable battery powers the system. The SIR-3000 weighs about 4.1 kg (9 lbs) and is backpack portable. The center frequency of the antenna used in this investigation is 200 MHz. With an antenna, the SIR-3000 typically requires two people to operate. Daniels (2004) and Jol (2008) discuss the uses and operation of GPR.

The RADAN for Windows (version 6.6) software program (GSSI) was used to process the radar records shown in this report.¹ Processing included: header editing, setting the initial pulse to time zero, color table and transformation selection, distance normalization, range gain adjustments, signal stacking, and migration, (see Daniels (2004) and Jol (2008) for discussions of these techniques). In addition, all radar records were subjected to surface normalization. Surface normalization corrects the radar record for changes in elevation. This processing technique greatly improves interpretations and the association of subsurface reflectors with landscape components. As elevation data were collected

¹ Manufacturer's names are provided for specific information; use does not constitute endorsement.

at a limited number of equally spaced points along each traverse line, depending on the local relief, the accuracy of the geodetic data will vary. As a consequence, surface normalized data should be viewed as close approximations of reality.

Data collected with GPR approximates, but slightly distorts the geometry of subsurface features and interfaces. This distortion is caused by the volumetric nature and spatial integration of subsurface information by antennas, and shifts in reflected data (Beck and Osborn, 1991). The radiation pattern of a radar antenna is analogous to that of a flashlight: radiation is conical (expanding horizontally with increasing distance or depth) with energy focused along the center of the beam and decreasing rapidly with distance away from the center of the beam. As a consequence, subsurface data collected with an antenna represents reflections from all interfaces within the relatively unfocused antenna's beam or *footprint area* (which expands with increasing depth). Migration is used to reduce this distortion and to improve interpretations. Migration is a processing technique that moves dipping reflectors to their "more correct" subsurface positions and collapses hyperbolic diffraction tails, which can obscure other subsurface interfaces (Geophysical Survey Systems, Inc., 2007). All radar records were migrated using Kirchhoff migration, which is sensitive to variations in migration velocity (Lehmann and Green, 2000). However, miscalculations in migration velocity estimates will result in some poorly positioned and focused images. Data were migrated prior to surface normalization to reduce distortion. Lehmann and Green (2000) observed that topographical migration should be considered in areas having slope gradients greater than 10 %.

Survey Procedures:

In each watershed, GPR traverses were completed along survey lines established across different landscape components. Survey flags were inserted in the ground at an interval of either 2- or 3-m along each line and served as reference points. Along each line, as the antenna was moved passed each reference point, a vertical mark was impressed on the radar record. These marks referenced known antenna positions on the radar records. The relative elevations of these positions were obtained with an engineering level and stadia rod. The establishment of these lines and collection of elevation data at each reference point along these lines required more time than the actual radar surveys. Moving the 200 MHz antenna along each traverse line completed a GPR traverse.

Terrain conditions within the two watershed provided uncommon obstacles for the radar surveys. Because of logistic and technical problems, GPR surveys are infrequently conducted across "topographically rugged terrains" (Heincke et al., 2005). Radar surveys conducted in "topographically rugged terrains" are daunting, fatiguing, and time consuming exercises. In addition to the challenges confronted in data collection, the processing and interpretation of the collected data are more complicated and demanding (Heincke et al., 2005). Forested conditions caused additional challenges to the radar work. Because of abrupt topographical changes and variations in the speed of antenna advance resulted in some changes in signal amplitudes and reflection characteristics. These survey artifacts are caused by variations in antenna-ground coupling and gaps or snags in radar records caused by rocks and vegetation.

Radar traverses were conducted either in a down slope or west to east directions. Because of very steep slopes, all radar surveys required three people (one to control the radar unit, one to direct and guide the antenna, and one to slow and steady the often downward movement of the antenna). Because footings were often insecure and the antenna difficult to handle, steep and forested terrains limit the speed and accuracy of GPR surveys. There was no "trial" or "dry runs" under these inhospitable and fatiguing terrain conditions. Only one pass with the GPR was made along each traverse line. Terrain conditions within these two watersheds were the most difficult and challenging that I have experienced in my near thirty-year career with GPR.

Table 2 summarizes the traverses that were conducted within the Alsea Watershed. For each radar record a file number is assigned. For each radar file, the identity of the traverse line, its length, interval between reference points, and general orientation is provided. Radar surveys were conducted either from top to bottom for down slope lines, and from West to East for lines established orthogonal to the slope. Table 2 summarizes the traverses that were conducted within the Watershed 10. Within Watershed 10, with the exception of line 11, all radar traverses were conducted in a down slope direction. For all GPR traverse lines in Watershed 10, the interval between reference points was 2 m.

Table 2 Summary of GPR traverses completed with the Aalsea Watershed

Line #	File #	Length (m)	Interval (m)	Orientation to slope
A	3	39	3	Downslope
B	4	34	2	Orthogonal
C	5	8	2	Orthogonal
D	6	38	2	Orthogonal
E	7	28	2	Downslope
F	8	8	2	Orthogonal
G	9	8	2	Downslope
H	10	8	2	Downslope
I	11	20	2	Downslope

Table 3 Summary of GPR traverses completed with Watershed 10

Line #	File #	Length	Description
1	File 16	12	Long Traverse
2	File 17	6	Long Traverse
3	File 18	12	Long Traverse
4	File 19	6	Long Traverse
5	File 20	16	Long Traverse
6	File 21	14	Long Traverse
7	File 22	8	Long Traverse
8	File 14	12	Top of Watershed
9	File 15	4	Top of Watershed
10	File 23	6	SE of Instrumented site
11	File 24	4	SE of Instrumented site

Calibration of GPR:

Ground-penetrating radar is a time scaled system. The system measures the time that it takes electromagnetic energy to travel from an antenna to an interface (e.g., soil horizon, stratigraphic layer, bedrock) and back. To convert the travel time into a depth scale, either the velocity of pulse propagation or the depth to a reflector must be known. The relationships among depth (D), two-way pulse travel time (T), and velocity of propagation (v) are described in the following equation (Daniels, 2004):

$$v = 2D/T \quad [1]$$

The velocity of propagation is principally affected by the relative permittivity (E_r) of the profiled material(s) according to the equation (Daniels, 2004):

$$E_r = (C/v)^2 \quad [2]$$

where “C” is the velocity of propagation in a vacuum (0.2998 m/nanosecond). Velocity is normally expressed in meters per nanosecond (ns). The velocity of propagation is slowed by increases in soil moisture and relative permittivity.

The velocity of propagation is spatiotemporally variable. Within both watersheds, soils were moist at the time of the GPR surveys. At each site, based on the depth to a buried reflector and hyperbola-matching procedures (the shape of a reflection (or diffraction) hyperbole is dependent on the velocity), an averaged velocity of propagation through the upper part of the soil profile was determined. At the Aalsea Watershed, based on the depth to a buried (50 cm) metal plate, the estimated velocity of propagation through the upper part of the soil profile was 0.0845 m/ns (E_r of 12.44). At Watershed 10, based on the depth to a buried (33 cm) metal plate, the estimated velocity of propagation through the upper part of the

soil profile was 0.0765 m/ns (E_r of 15.18). The radar record of the buried metallic reflector at the Alesa Watershed calibration site is shown in Figure 1.

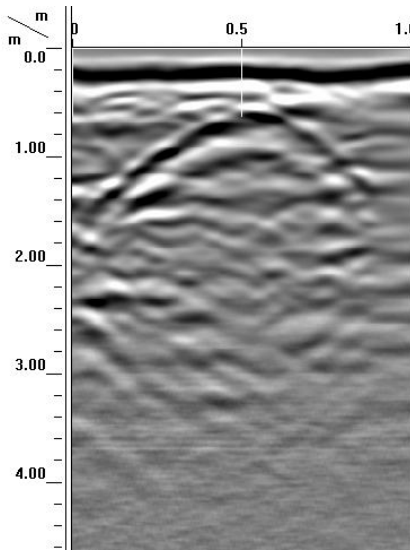


Figure 1. The hyperbola evident in the upper part of this radar record represents reflections from a metallic reflector that was buried at a depth of 50 cm within the Alesa Watershed.

It is recommended that multiple calibration tests be performed in each study area as velocities will change laterally and with depth. These variations are caused by changes in the water content of soils and parent rocks. In each watershed, it was assumed that the soils were moister than the underlying saprolite and unweathered bedrock. As a consequence, velocities of propagation were assumed to be lower and dielectric permittivities higher in the soil than in the underlying saprolite, and higher in the saprolite than in the underlying unweathered bedrock. As velocity estimates and depth calibrations were only based on the depths to one, very-shallowly buried object in each watershed, all depth scales should be considered as mere *ballpark estimates*. At a later time, if depths to lower-lying subsurface interfaces can be confirmed through core observations and these features can be associated with reflections on radar records, estimates and relative depth scales can be improved.

On radar records, reflections from interfaces spaced closer than one-half wavelength apart are indistinguishable due to constructive and destructive interference (Daniels, 2004). Daniels (2004) used the following equation to show the relationship between velocity of propagation (v), antenna center frequency (f), and wavelength (λ):

$$\lambda = v/f \quad [3]$$

Equation [3] shows that the propagated wavelength will decrease with decreasing propagation velocity and increasing antenna frequency. For a given frequency, propagation velocity and wavelength will decrease with increasing E_r . Based on equation [3] and the estimated velocity of pulse propagation, the estimated wavelengths for the 200 MHz antenna are about 42 and 38 cm within the Alesa and H. J. Andrews Watersheds, respectively. In general, interfaces spaced closer (vertically) than $\frac{1}{2}$ a wavelength will be combined and can not be individually recognized on radar records. As a consequence, with the 200 MHz antenna, subsurface interfaces must be spaced greater than about 19 to 22 cm to be distinguished on radar records within these watersheds.

Background:

In the absence of continuous and satisfactory outcrops or exposures, GPR is an accepted tool for imaging the regolith (Dagallier et al., 2000; and Beres and Haeni, 1991). Ground-penetrating radar has been used extensively to chart bedrock depths (Collins et al., 1989; Davis and Annan, 1989), changes in rock type (Davis and Annan, 1989), fractures and joint

patterns (Theune et al., 2006; Porsani et al., 2005; Nascimento da Silva et al., 2004; Pipan et al., 2000;) and faults (Demagnet et al., 2001). It has been used to detect geologic hazards in advance of mining operations (Singh and Chauhan, 2002; Grodner, 2001; and Molinda et al., 1996), and to optimize the quality and homogeneity of quarried ornamental stone blocks (Kadioglu, 2008; Porsani et al., 2006; and Grandjean and Gourry, 1996). GPR has been used to locate and characterize faults and fracture patterns in rock (Patidar et al., 2007; Lane et al., 2000; Grasmueck, 1996; Stevens et al., 1995; Toshioka et al., 1995; and Holloway and Mugford, 1990) and cavities, sinkholes, and fractures in limestone (Al-fares et al., 2002; Pipan et al., 2000; and Barr, 1993). Recent improvements in data processing, which allow the construction of three-dimensional radar pseudo-images, have been used to improve the characterization of rock structure and geometry (Corbeau et al., 2001b; Szerbiak et al., 2001; Beres et al., 2000; Junck and Jol, 2000; and McMechan et al., 1997).

Ground-penetrating radar has been used to study weathered bedrock and the transition from weathered to hard bedrock (Porsani et al., 2006; Hubbert et al., 2001; Volkel et al., 2001; and Li, 1998). Porsani et al. (2006) related reflectors that paralleled the surface to the contact between weathered and unweathered granite. Aranha et al. (2002) used GPR to study highly weathered soil profiles and saprolite in the humid sub-tropics of Brazil. In their study, differences in signal amplitude and reflection patterns were used to distinguish saprolite from overlying colluvium. Beauvais et al. (2003) used GPR to characterize ferricrete and soft ferricrete horizons in deeply weathered soils of eastern Senegal. In these soils, horizons with different Fe_2O_3 , kaolinite clay content, and/or porosity were detected with GPR to depths of 5 to 10 m.

Bedrock restricts, redirects and concentrates the flow of water. Ground-penetrating radar has been used in hydrogeologic investigations to study the structure (fractures, unloading or exfoliation joints, bedding and stress planes, cavities, etc.) of different rocks (Theune et al., 2006; Porsani et al., 2005; Al-fares et al., 2002; Singh and Chauhan, 2002; Beres and Haeni, 1991). Singh and Chauhan (2002) used GPR and geologic data to characterize limestone at a mining operation. Radar data were used to estimate limestone extraction depths without the possibility of excessive seepage from highly fractured or weathered sections of the bedrock. Al-fares et al. (2002) used GPR to assess conduits in fractured and karstified limestone. Their study revealed structural features (e.g., bedding and fracture planes, karstified zones, compacted and massive limestone, conduits), which influenced the infiltration of water. Porsani et al. (2005) used GPR to characterize aquifers in fractured granite and trace highly inclined fractures, which were infilled with water and/or weathered materials, to depths as great as 30 m. High amplitude radar reflections are associated with water-filled bedding planes, joints, and fractures (Buursink and Lane, 1999; Olhoeft, 1998; Grasmueck, 1994). In the aforementioned hydrogeologic studies, GPR was used to characterize bedding and fracture planes, but provided little information on existing subsurface circulation patterns. However, in a study conducted by Porsani et al. (2005), the location of fractures did aid the location of wells for the extraction of potable water.

In rocks, GPR reflections are produced by bedding, cleavage, and fracture planes. Reflections are produced at interfaces separating features with different lithologic properties (density, porosity, grain size, clay content, etc.) and water contents (Corbeau et al., 2001a). Contacts separating different lithologic units have been identified by differences in signal amplitudes, reflection patterns (continuity and geometric configurations) and the termination of reflections (Corbeau et al., 2001b). In bedrock, variations in dielectric properties are principally associated with changes in water content (Davis and Annan, 1989). Abrupt changes in water content produce strong radar reflections. Saturated fractures and bedding planes will produce reflections with higher-amplitude than similar air-filled or unsaturated features (Lane et al., 2000).

Because of scattering losses, signal attenuation, wave-length scale heterogeneities, and geometric constraints, the number of bedding and fractures planes interpreted on radar records are considered to be an order of magnitude less than the number observed in outcrops (Lane et al., 2000). Closely spaced bedding and fracture planes can produce reverberations that can mask other reflections. Lane et al. (2000) observed that fractures spaced closer than $\frac{1}{4}$ of the transmitted wave length were obscured by constructive interference.

Larger dip-angles and/or more irregular surfaces will also increase the scattering of the reflected wave-front away from the antenna. Vertical interfaces reflect very little energy towards the antenna. Fractures and bedding planes with dip-angles greater than about 45 degrees are affected by spatial aliasing distortion and can not be accurately imaged with GPR (Buursink and Lane 1999; Ulriksen, 1982). However, Orlando (2002) found that steep or nearly vertical fractures are detectable when they have irregular geometry and are filled with finer-textured materials and water.

Results:

An aim of this study is to combine GPR, geomorphic, hydrologic and sedimentological and soil information in the study of small, steeply-sloping, forested watersheds. Despite the inhospitality of these terrains, GPR traverses were completed and some subsurface information was obtained to estimated depths of about 5 m. On radar records, contrasting subsurface materials and layers are suggested by abrupt change in signal scattering, amplitude strengths, and reflection patterns. As an example, the presence of contrasting layers and materials is evident on the radar record shown in Figure 2. Figure 2 contains two renditions of Traverse A from the Alsea Watershed. On each radar record, the vertical and horizontal scales are expressed in meters. The selected color table and transformation reflects the preference of this user. The horizontal scale has been adjusted through *distance normalization*, which establishes a constant scale between each reference mark (spaced 3-m apart). The vertical scale has been adjusted for changes in surface elevation (measured at each reference points) through *surface normalization*. Through *surface normalization*, subsurface reflectors more closely approximate their true geometry and relationship to the soil surface. In addition, the radar record shown in Figure 2 has been migrated.

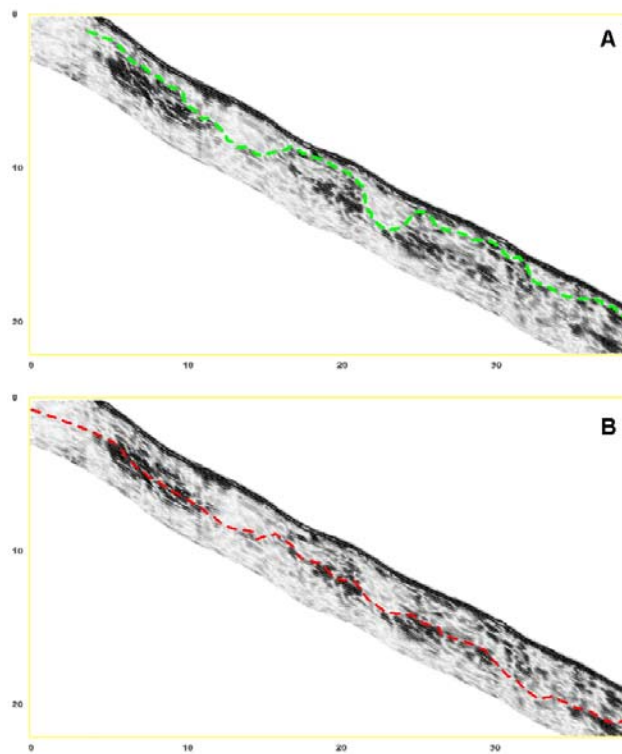


Figure 2. On this radar record from the Alsea Watershed, two alternative interpretations of a subsurface interface are provided. In the absence of ground truth verifications, both interpretations are assumed to be equally valid at this time.

With GPR it is possible to obtain information that can aid the identification and delineation of different subsurface units and characterize their internal structure. The complexity of the subsurface is evident in the radar record shown in Figure 2. Subsurface interfaces representing layers of contrasting materials are evident on this radar record. These interfaces are numerous, segmented, and variable in expression and amplitude. Because of gaps in the reflection patterns and variations in the amplitudes of reflected signals, these interfaces are difficult to trace laterally with a high degree of confidence. The upper and lower radar records show two different possible interpretations of a major interface that occurs within the subsurface. In the absence of adequate ground truth core data, neither interpretation can be confirmed. These two renditions of the same radar record are shown to help emphasize the subjective nature of GPR interpretations and the need for cautious explanations of interpretative results. The depth (vertical) scale shown in these renditions is an approximation based on a single calibration point and for soil properties existing within depths of less than 50 cm. Soils were moist at the time of this investigation. Because of the relatively high soil moisture contents, the estimated Er is

higher and the v slower than anticipated for the underlying saprolite and unweathered parent rock. The depth scale should therefore be considered a *conservative, ball-park estimate*, which probably underestimated the depths to features within the presumably (my belief) better drained, underlying lithology.

In Figure 2, because of the applied surface *normalization* processing procedures, the vertical scale is 1:4. This scale (1:4) results in the compression of the vertical (depth) scale by a factor of 4. As distances between reference points were measured on an incline along the soil surface, they do not represent true horizontal distances. The *sine qua non* is that the radar records shown in this report are all distorted and exaggerated, and should only be considered close approximations of true forms.

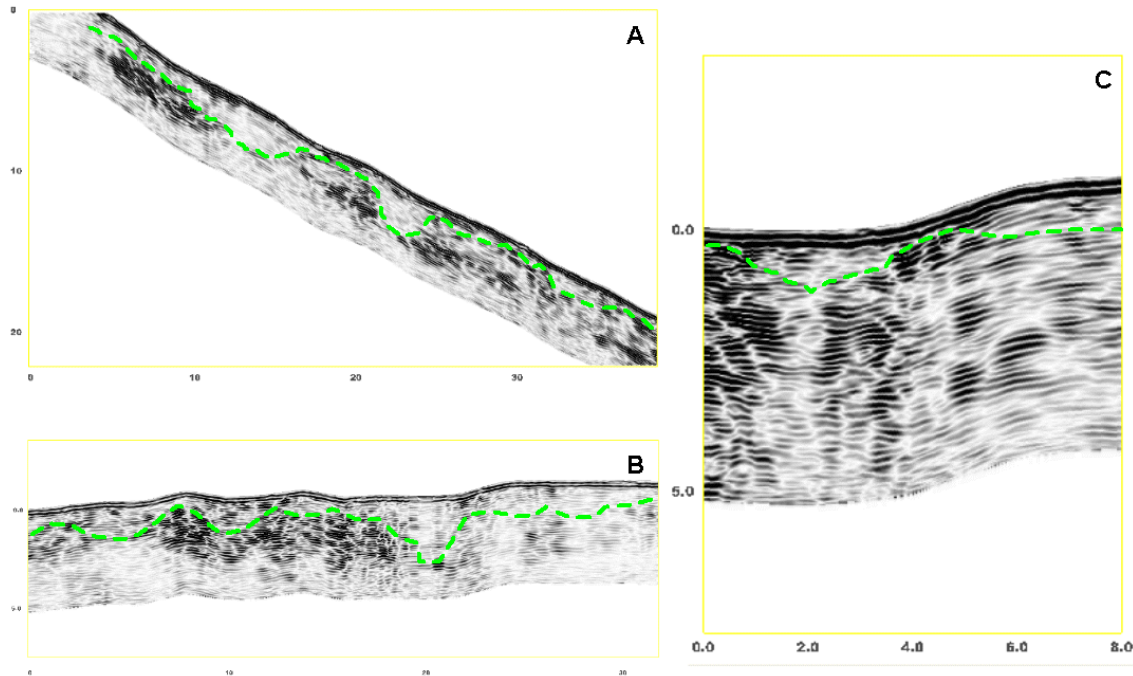


Figure 3. Three GPR records collected on higher-lying slope component within the Alsea Watershed. On each radar record a green-colored, segmented line has been used to identify the interpreted soil-bedrock interface.

Figure 3 contains three radar records from traverses that were conducted on higher-lying slopes within the Alsea Watershed. In each radar record, the horizontal and vertical scales are expressed in meters. The lettering in the upper right-hand corner of each radar record identifies the traverse line (see Table 2). Green-colored lines have been used to approximate a major subsurface interface. This interface is believed to represent the contact between the soil and the underlying parent rock. In the two investigated watersheds, the parent rocks consist of an upper weathered zone (saprolite, Cr horizon), which overlies a relatively unweathered zone (R horizon).

Saprolite consists of decomposed rock that has weathered in place and is characterized by preservation of original rock structure, foliation, and jointing (Pavich et al., 1989). Saprolite is found in landscapes where rocks have been exposed to weathering processes for long periods of time. The thickness of saprolite varies with lithology and topographic position (Buol and Weed, 1991; Daniels and Hammer, 1992). In eastern USA, saprolite has been observed to be thinner over mafic and ultramafic rocks and on steep slopes where erosion is most severe (Pavich et al., 1989). In northern Virginia, saprolite is generally thickest over quartzofeldspathic rocks and on less sloping and more stable surfaces (Pavich et al., 1989). Pavich et al. (1989) reported that “the contacts between weathered and unweathered rock are typically gradational, highly irregular, and difficult to define precisely”. As GPR is best suited for the detection of abrupt and highly contrasting layers, the gradational nature of the contacts between weathered and unweathered rock is considered generally unfavorable to GPR.

Figure 4 contains four radar records from traverses that were conducted on lower-lying slopes within the Alesa Watershed. In each radar record, the horizontal and vertical scales are expressed in meters. The lettering in the upper right-hand corner of each radar record identifies the traverse line (see Table 2). Green-colored lines have been used to approximate a major subsurface interface. This interface is presumed to represent the contact between the soil and the underlying parent rock. While the contact can be identified with some degree of confidence, the weathering state of the underlying rock can not be properly interpreted. If the materials underlying the soils are saprolite, variations in the expression of the soil-saprolite interface should reflect differences in the abruptness and contrast (which ultimately reflects differences in weathering) across this contact.

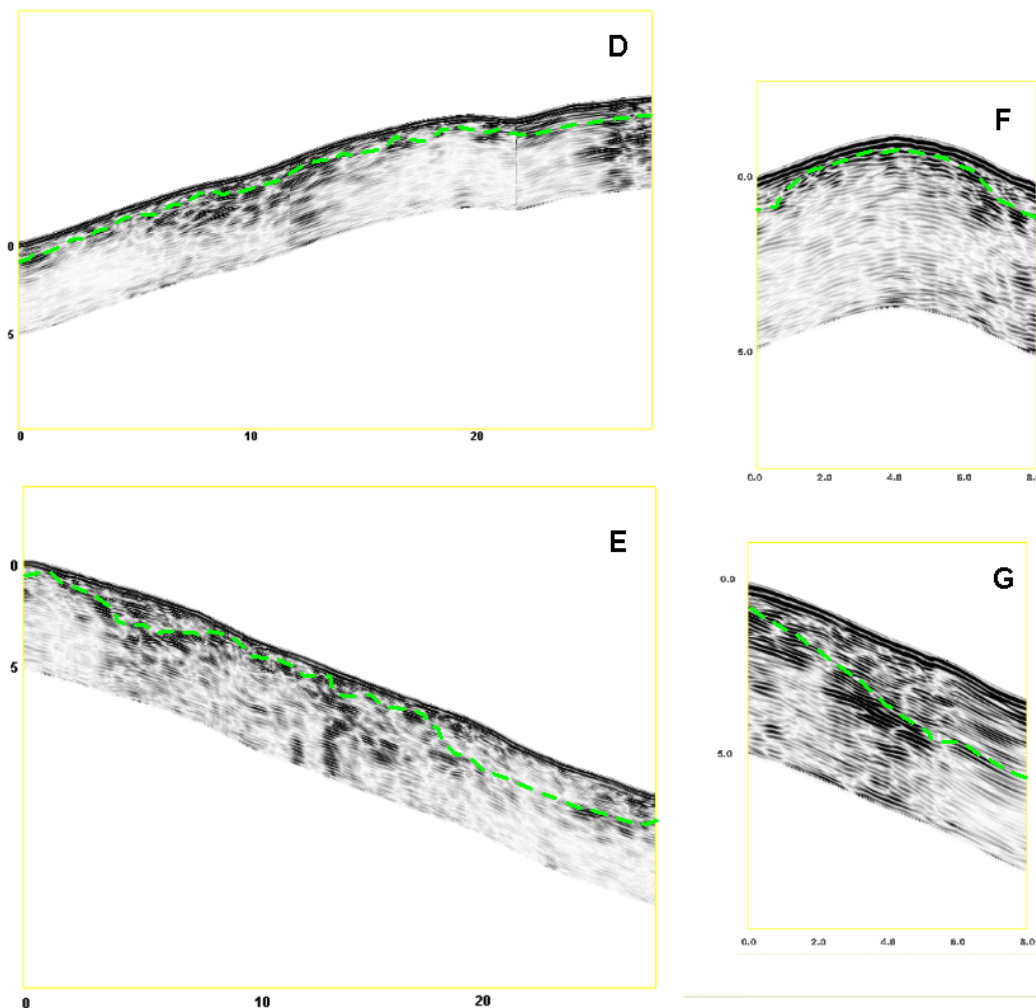


Figure 4. GPR records collected on lower-lying slope component in the Alesa Watershed. On each radar record a green-colored, segmented line has been used to identify the interpreted soil-bedrock interface.

In the surface normalized radar records shown in Figure 4, below what is perceived as the soil-bedrock interface (green-colored lines), zones of varying signal amplitudes alternate with zones of apparently no signal return. The zones of no signal return are interpreted as consisting of relatively homogenous materials or layers that have slight and imperceptible (to GPR) differences in dielectric properties. One possible interpretation is that these zones represent differences in the intensity of weathering with discontinuous layers or pockets of more- or less-intensely weathered bedrock extending to different depths. Beauvais et al. (2003) associated anomalous areas with obvious disruptions or the absence of reflections to saprolite. In each radar record shown in Figure 4, zones of constructive and destructive signal interference suggest possible fracturing in the bedrock. Porsani et al. (2006) interpreted deeper zones of no signal returns on radar records as representing homogenous, unfractured and relatively unweathered granite rock.

Figure 5 contains two radar records from traverses that were conducted on lower-lying slopes within the Alsea Watershed. In each radar record, the horizontal and vertical scales are expressed in meters. The lettering in the upper right-hand corner of each radar record identifies the traverse line (see Table 2). Traverse line H extends down a steep side slope and ends along the stream channel. Red-colored lines have been used to approximate a major subsurface interface; presumably the soil-bedrock contact. The deeper portions of each radar record lack high-amplitude radar reflections. This could reflect (1) more conductive (higher clay and/or moisture contents), over-lying materials and higher rates of signal attenuation, which would limit penetration depths; or (2) more homogenous materials, which lack contrasting layers (if bedrock is more saturated with water, the increased water content may increase signal attenuation rates and mask differences between layers).

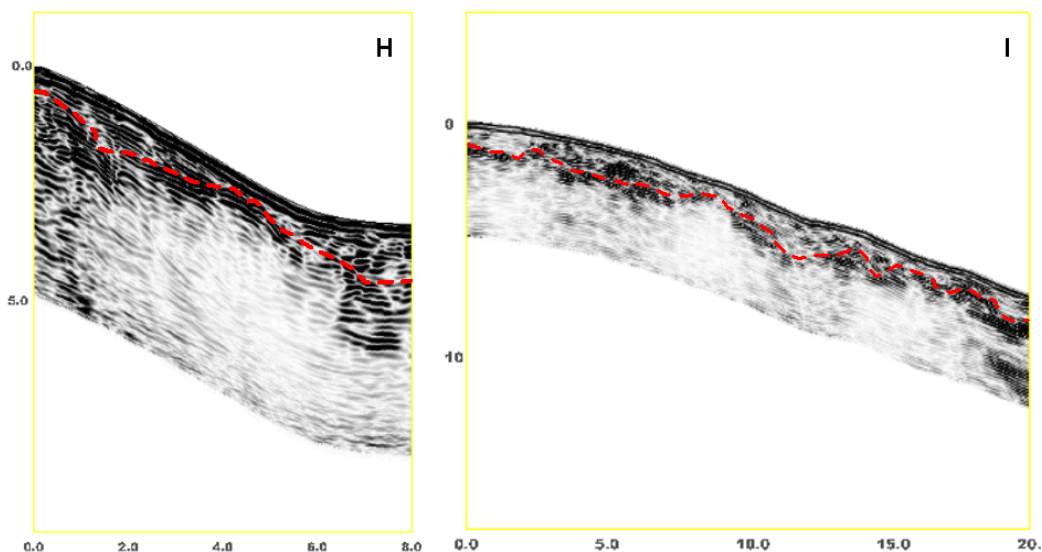


Figure 5. Additional GPR records collected on lower-lying slope component in the Alsea Watershed. On each radar record a red-colored, segmented line has been used to identify the interpreted soil-bedrock interface.

Figure 6 contains two radar records from traverses that were conducted on the summit area to the Watershed 10 in the H. J. Andrews. Experimental Forest. In each radar record, the horizontal and vertical scales are expressed in meters. The numbers in the upper right-hand corner of each record identify the traverse lines (see Table 3). Traverse lines 8 and 9 were both conducted in down slope directions. Red-colored lines have been used to approximate a major subsurface interface that is believed to represent the soil-bedrock contact. A green-colored line has been used to identify a deeper, prominent, continuous subsurface reflector on traverse line 8. Differences in signal amplitudes that are evident between these two radar records are caused by differences in gain functions used to display each file. On both radar records, alternating subsurface patterns with variable signal amplitudes and diverse geometries suggest non-uniform spatial weathering intensities and associated features.

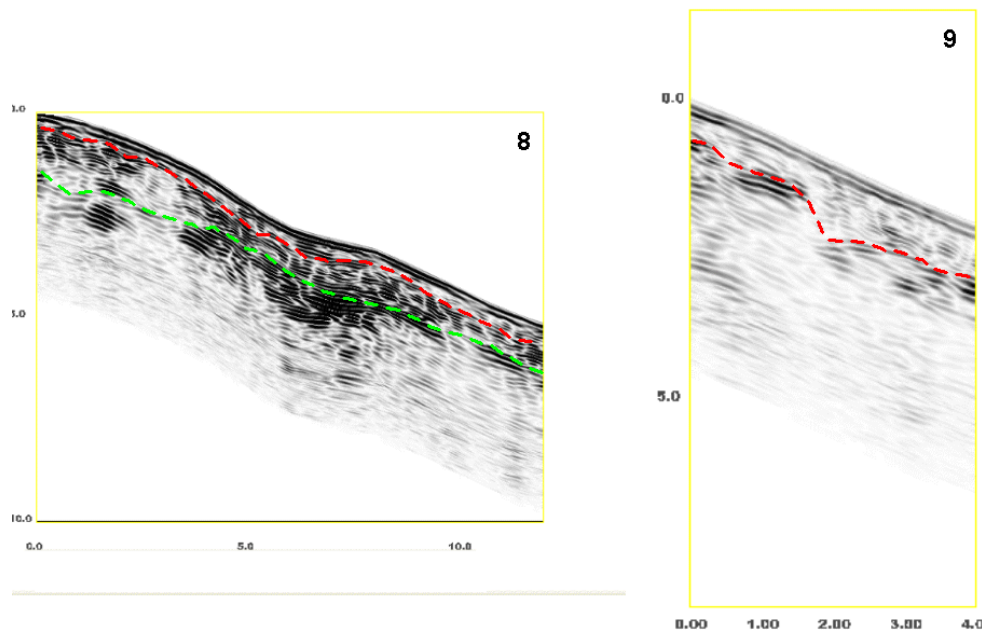


Figure 6. These two radar records were collected on a summit area in Watershed 10 at the H.J. Andrews Experimental Forest. On each radar record a red-colored, segmented line has been used to identify the interpreted soil-bedrock interface.

Figure 7 contains four radar records, which were collected in sequence (1→2→3→4) as the 200 MHz antenna was moved down a side slope in Watershed 10. In each radar record, the horizontal and vertical scales are expressed in meters. The numbers in the upper right-hand corner of each record identify the traverse lines (see Table 3). Red-colored lines have been used to approximate a major subsurface interface that is believed to represent the soil-bedrock interface. These radar records serve to illustrate the variability of the subsurface over short distances within this watershed.

Ground-penetrating radar (GPR) can be used to detect and characterize some fractures in rocks. For a given antenna frequency, the detection of fractures is dependent on the width of the discontinuity and the nature of the in-filled materials (fractured in-filled with water or moist soil materials provide higher amplitude reflections and are more easily identified than air filled fractures). Truncations in the lateral continuity of planar reflectors, which are cut by often tortuous, vertical patterns, are suggests the locations of some small-scale inhomogeneities and/or fractures in bedrock. As noted by Sassen and Everett (2009), depending on the width, the nature of the in-filled materials, and the orientations of fractures, these features will alters the incident waveform or wave shape of a GPR signal through constructive and destructive interference. Though not confirmed, constructive and destructive interference is believed to be partially responsible for the segmentation of interfaces and the appearance of tortuous, white-colored, downward descending vertical patterns on these radar records. Similar vertical patterns have been observed in fractured bedrock (Jeannin et al., 2006; Porsani et al., 2006; Nascimento da Silva et al., 2004). A noticeable group of closely spaced vertical fractures are suggested in the area enclosed by a green-colored rectangle in Traverse line 3. However, similar patterns are distinguishable on all radar records collected within this and the Alesa Watersheds. These patterns may by qualitatively used to infer the presence of discontinuities, which are inferred to represent fractures and potential ground water flow paths.

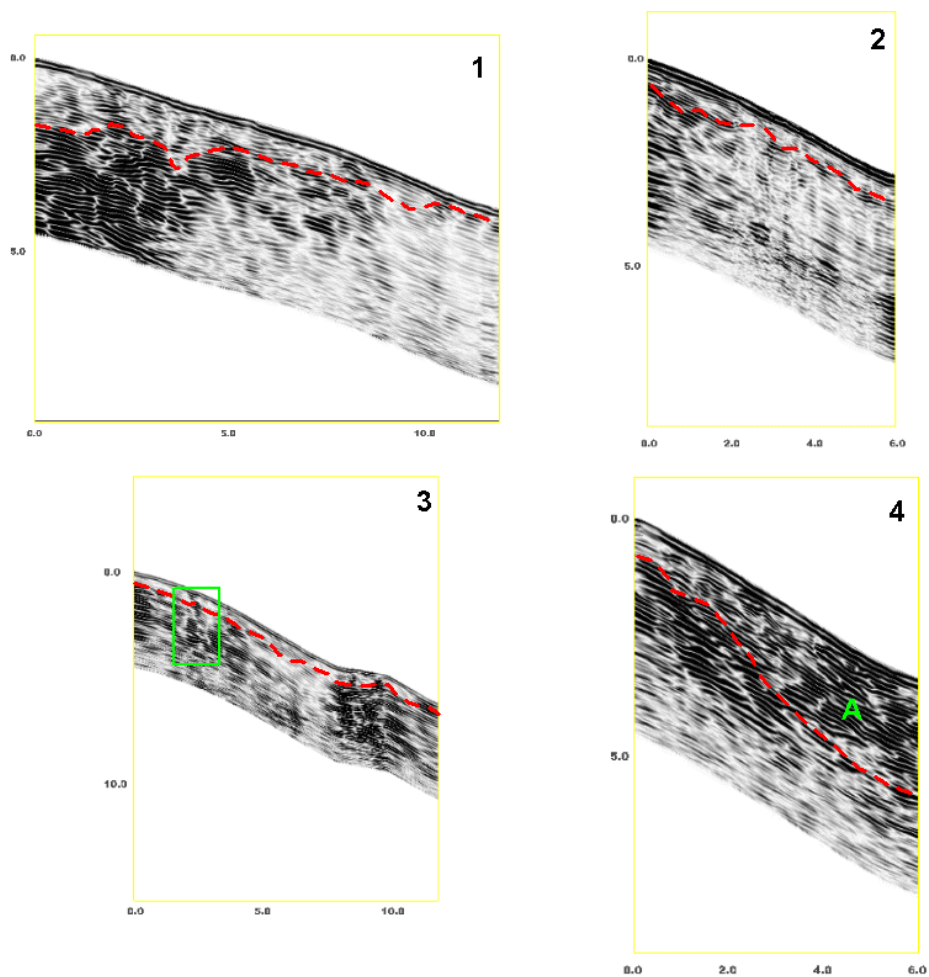


Figure 7. A sequence of radar records of different lengths collected along a steeply sloping, forested side slope in Watershed 10. On each radar record a red-colored, segmented line has been used to identify the interpreted soil-bedrock interface.

References:

- Al-fares, W., M. Bakalowicz, R. Guerin, and M. Dukhan, 2002. Analysis of the karst aquifer structure of the Lamalou area (Herauld, France) with ground penetrating radar. *Journal of Applied Geophysics* 51: 97-106.
- Aranha, P. R. A., C. H. R. R. Augustin, and F. G. Sobreira, 2002. The use of GPR for characterizing underground weathered profiles in the sub-humid tropics. *Journal of Applied Geophysics* 49: 195-210.
- Barr, G. L., 1993. Application of ground-penetrating radar methods in determining hydrogeologic conditions in a karst area, west-central Florida. USGS Water Resources Report 92-4141. Tallahassee, Florida. 26 p.
- Beauvais, A., M. Ritz, J.-C. Parisot, C. Bantsimba, and M. Dukhan, 2003. Combined ERT and GPR methods for investigating two-stepped lateritic weathering systems. *Geoderma* 119 (1-2):121-132.
- Beck, R., and J. Osborn, 1991. Three-dimensional migration and forward modeling of ground penetrating radar data. Report Number CMU-RI-TR-91-12. The Robotic Institute, Carnegie Mellon University, Pittsburgh, PA.

- Beres, M., A. G. Green, and A. Pugin, 2000. Diapiric origin of the Chessel-Noville Hills of the Rhone Valley interpreted from georadar mapping. *Environmental and Engineering Geoscience* 6(2): 141-153.
- Beres, M., and F. P. Haeni, 1991. Application of ground-penetrating-radar methods in hydrogeologic studies. *Ground Water* 29(3): 375-386.
- Buol, S. W., and S. B. Weed, 1991. Saprolite-soil transformation in the Piedmont and mountains of North Carolina. *Geoderma* 51: 15-28.
- Buursink, M. L., and J. W. Lane, 1999. Characterizing fractures in a bedrock outcrop using ground-penetrating radar at Mirror Lake, Grafton County, New Hampshire. 769-776 pp. IN: Morganwalp, D.W., and Buxton, H.T. (eds.), U.S. Geological Survey Toxic Substances Hydrology Program--Proceedings of the Technical Meeting, Charleston, South Carolina, March 8-12, 1999--Volume 3 of 3--Subsurface Contamination from Point Sources: U.S. Geological Survey Water-Resources Investigations Report 99-4018C.
- Collins, M. E., J. A. Doolittle, and R. V. Rourke, 1989. Mapping depth to bedrock on a glaciated landscape with ground-penetrating radar. *Soil Science Society of America Journal* 53(3): 1806-1812.
- Corbeanu, R. M., G. A. McMechan, R. B. Szerbiak, and K. Soegaard, 2001a. Prediction of 3-D fluid permeability and mudstone distributions from ground-penetrating radar attributes: Example from the Cretaceous Ferron sandstone member, east-central Utah. *Geophysics* 67(5): 1495-1504.
- Corbeanu, R. M., K. Soegaard, R. B. Szerbiak, J. B. Thurmond, G. A. McMechan, D. Wang, S. Snelgrove, C. B. Forster, and A. Menitove, 2001b. Detailed internal architecture of fluvial channel sandstone determined from outcrop, cores and 3-D ground-penetrating radar: Example from the middle Cretaceous Ferron sandstone, east-central Utah. *American Association of Petroleum Geologists Bulletin* 85(9): 1583-1608.
- Dagallier, G., A. I. Laitinen, F. Malartre, I. P. Van Campenhout, and P. C. H. Veecken, 2000. Ground penetrating radar application in a shallow marine Oxfordian limestone sequence located on the eastern flank of the Paris Basin, NE France. *Sedimentary Geology* 130: 149-165.
- Daniels, D. J., 2004. *Ground Penetrating Radar; 2nd Edition*. The Institute of Electrical Engineers, London, United Kingdom.
- Daniels, R. B., and R. D. Hammer. 1992. *Soil Geomorphology*. John Wiley & Sons, Inc. New York, New York.
- Davis, J. L., and A. P. Annan, 1989. Ground-penetrating radar for high-resolution mapping of soil and rock stratigraphy. *Geophysical Prospecting* 37: 531-551.
- Demant, D., L. G. Evers, H. Teerlynck, B. Dost, and D. Jongmans, 2001. Geophysical investigations across the Peel boundary fault (The Netherlands) for a paleoseismological study. *Netherlands Journal of Geosciences* 80 (3-4): 119-127.
- Geophysical Survey Systems, Inc., 2007. RADAN 6.5 User's Manual. Geophysical Survey Systems, Inc., Salem, New Hampshire.
- Grandjean, G., and J. C. Gourry, 1996. GPR data processing for 3D fracture mapping in a marble quarry (Thassos, Greece). *Journal of Applied Geophysics* 36: 19-30.
- Grodner, M., 2001. Using ground penetrating radar to quantify changes in fracture pattern associated with a simulated rockburst experiment. *Journal of the South African Institute of Mining and Metallurgy*. Vol. 101(5): 261-266.
- Grasmueck, M., 1996. 3-D ground-penetrating radar applied to fracture imaging in gneiss. *Geophysics* 61(4): 1050-1064.

- Grasmueck, M., 1994. Application of seismic processing techniques to discontinuity mapping with ground-penetrating radar in crystalline rock of the Gotthard Massif, Switzerland. 1135-1149 pp. In *Proceeding of the Fifth International Conference on Ground Penetrating Radar*. Waterloo Centre for Groundwater Research and Canadian Geotechnical Society. June 12-16 1994, Kitchner, Ontario, Canada.
- Heincke, B., A. G. Green, J. van der Kruk, and H. Horstmeyer, 2005. Acquisition of and processing strategies for 3D georadar surveying a region characterized by rugged topography. *Geophysics* 70(6): k53-k61.
- Holloway, A. L., and J. C. Mugford, 1990. Fracture characterization in granite using ground probing radar. *CIM Bulletin* 83 (940): 61- 70.
- Hubbert, K. A., R. C. Graham, and M. A. Anderson, 2001. Soil and weathered bedrock: components of a Jeffrey pine plantation substrate. *Soil Science Society of America Journal* 65:1255-1262.
- Jeannin, M., S. Garambois, C. Grégoire, and D. Jongmans, 2006. Multiconfiguration GPR measurements for geometric fracture characterization in limestone cliffs (Alps). *Geophysics* 71(3): B85-B92.
- Jol, H., 2008. *Ground Penetrating Radar: Theory and Applications*. Elsevier Science, Amsterdam, The Netherlands.
- Junck, M. B., and H. M. Jol, 2000. Three-dimensional investigation of geomorphic environments using ground penetrating radar. 314-318 pp. IN: (Noon, D. ed.) *Proceedings Eight International Conference on Ground-Penetrating Radar*. May 23 to 26, 2000, Gold Coast, Queensland, Australia. The University of Queensland.
- Kadioglu, S., 2008. Photographing layer thickness and discontinuities in a marble quarry with 3D GPR visualization. *Journal of Applied Geophysics* 64: 109-114.
- Lane, J. W., M. L. Buursink, F. P. Haeni, and R. J. Versteeg, 2000. Evaluation of ground-penetrating radar to detect free-phase hydrocarbons in fractured rocks – results of numerical modeling and physical experiments. *Ground Water* 38(6): 929-938.
- Lehmann, F., and A. G. Green, 2000. Topographic migration of georadar data: Implications for acquisition and processing. *Geophysics* 65(3): 836-848.
- Li, Z., 1998. Applications of ground penetrating radar in Three Gorges Project. 209-213 pp. IN: (Plumb, R. G., ed.) *Proceedings Seventh International Conference on Ground-Penetrating Radar*. May 27 to 30, 1998, Lawrence, Kansas. Radar Systems and Remote Sensing Laboratory, University of Kansas.
- McMechan, G. A., G. C. Gaynor, and R. B. Szerbiak, 1997. Use of ground-penetrating radar for 3-D sedimentological characterization of clastic reservoir analogs. *Geophysics* 62(3): 786-796.
- Molinda, G. M., W. D. Monaghan, G. L. Mowrey, and G. F. Persetic, 1996. Using ground penetrating radar for roof hazard detection in underground mines. USDOE. Pittsburgh Research Center, RI 9625.
- Nascimento da Silva, C. C., W. E. de Medeiros, E. F. Jarmin de Sa, and P. X. Neto, 2004. Resistivity and ground-penetrating radar images of fractures in a crystalline aquifer: a case study in Caicara farm – NE Brazil. *Journal of Applied Geophysics* 56: 295-307.
- Olhoeft, G., 1998. Electrical, magnetic, and geometric properties that determine ground penetrating radar performance. 177-182 pp. IN: Plumb, R. G. (ed.) *Proceedings of the Seventh International Conference on Ground-Penetrating Radar*. May 27 to 30, 1998, Lawrence, Kansas. Radar Systems and Remote Sensing Laboratory, University of Kansas.
- Orlando, L., 2002. Ground penetrating radar in massive rock: A case history. *First Break* 20 (7): 467-471

- Patidar, A. K., D. M. Maurya, M. G. Thakkar, and L. S. Chamyal, 2007. Fluvial geomorphology and neotectonic activity based on field and GPR data, Katrol hill range, Kachchh, Western India. *Quaternary International* 159: 74-92.
- Pipan, M., L. Baradello, E. Forte, and A. Prizzon, 2000. GPR study of bedding planes, fractures and cavities in limestone. 682-687. IN: (Noon, D. ed.) Proceedings Eight International Conference on Ground-Penetrating Radar. May 23 to 26, 2000, Gold Coast, Queensland, Australia. The University of Queensland.
- Pavich, M. J., G. W. Leo, S. F. Obermeier, and J. R. Estabrook. 1989. Investigations of the characteristics, origin, and residence time of the upland residual mantle of the Piedmont of Fairfax County, Virginia. U.S. Geol. Survey Prof. Paper No. 1352.
- Porsani, J. L., V. R. Elis, and F. Y. Hiodo, 2005. Geophysical investigations for the characterization of fractured rock aquifer in Itu, SE Brazil. *Journal of Applied Geophysics* 57: 119-128.
- Porsani, J. L., W. A. Sauck, and A. O. S. Junior, 2006. GPR for mapping fractures and as a guide for the extraction of ornamental granite from a quarry: A case study from southern Brazil. *Journal of Applied Geophysics* 57 (2): 119-128
- Sassen, D.S., and M. E. Everett, 2009. 3D polarimetric GPR coherency attributes and full-waveform inversion of transmission data for characterizing fractured rock. *Geophysics* 74 (3): J23-J34.
- Singh, K. K. K., and R. K. S. Chauhan, 2002. Exploration of subsurface strata conditions for a limestone mining area in India with ground-penetrating radar. *Environmental Geology* 41: 966-971.
- Stevens, K. M., G. S. Lodha, A. L. Holloway, and N. M. Soonawala, 1995. The application of ground penetrating radar for mapping fractures in plutonic rocks within the Whiteshell Research Area, Pinawa, Manitoba, Canada. *Journal of Applied Geophysics* 33: 125-141.
- Szerbiak, R. B., G. A. McMechan, R. Corbeanu, C. Forster, and S. H. Snelgrove, 2001. 3-D characterization of a clastic reservoir analog: from 3-D GPR data to a 3-D fluid permeability model. *Geophysics*, 66(4): 1026-1037.
- Toshioka, T., T., Tsuchida, and K. Sasahara, 1995. Application of GPR to detecting and mapping cracks in rock slopes: *Journal of Applied Geophysics* 33: 119-124.
- Theune, U., D. Rokosh, M. D. Sacchi, and D. R. Schmitt, 2006. Mapping fractures with GPR: A case study from Turtle Mountain. *Geophysics* 71(5): B139-B150.
- Ulriksen, C. P. F., 1982. Application of impulse radar to civil engineering. Ph.D. dissertation. Lund University of Technology. Lund, Sweden.
- Volkel, J., M. Leopold, and M. C. Roberts, 2001. Demontre l'utilite du GPR comme outil pour la representation graphique des sediments des couches sous-jacentes. *Permafrost and Periglacial Processes* 12: 379-387.